Accepted for publication in ApJ
Preprint typeset using LaTeX style AASTeX6 v. 1.0

arXiv:1609.08174v1 [astro-ph.GA] 26 Sep 2016

REVERSED RADIAL DISTRIBUTION TREND OF SUBPOPULATIONS IN THE GLOBULAR CLUSTERS NGC 362 AND NGC 6723

Dongwook Lim[1], Young-Wook Lee[1], Mario Pasquato[1], Sang-Il Han[2], and Dong-Goo Roh[2]

[1]Center for Galaxy Evolution Research & Department Astronomy, Yonsei University, Seoul 03722, Korea; dwlim@galaxy.yonsei.ac.kr, ywlee2@yonsei.ac.kr

[2]Korea Astronomy and Space Science Institute, Daejeon 34055, Korea

ABSTRACT

Most globular clusters (GCs) are now known to host multiple stellar populations with different light element abundances. Here we use narrow-band photometry and low-resolution spectroscopy for NGC 362 and NGC 6723 to investigate their chemical properties and radial distributions of subpopulations. We confirm that NGC 362 and NGC 6723 are among the GCs with multiple populations showing bimodal CN distribution and CN-CH anti-correlation without a significant spread in calcium abundance. These two GCs show more centrally concentrated CN-weak earlier generation stars compared to the later generation CN-strong stars. These trends are reversed with respect to those found in previous studies for many other GCs. Our findings, therefore, seem contradictory to the current scenario for the formation of multiple stellar populations, but mass segregation acting on the two subpopulations might be a possible solution to explain this reversed radial trend.

Keywords: globular clusters: general — globular clusters: individual (NGC 362, NGC 6723) — stars: abundances — stars: evolution

1. INTRODUCTION

Recent observations suggest that most globular clusters (GCs) host multiple stellar populations showing star-to-star abundance variations in the light elements, such as C, N, O, Na and Al (e.g., Carretta et al. 2009; Gratton et al. 2012; Piotto et al. 2015, and references therein). Among several scenarios for the origin of these abundance variations, the most widely accepted one is the self-enrichment scenario, which explains these variations by the chemical pollution/enrichment from earlier generation stars, such as intermediate-mass asymptotic giant branch (IMAGB) stars (Ventura & D'Antona 2008), rotating AGB stars (Decressin et al. 2009), interacting binary stars (de Mink et al. 2009), and fast-rotating massive stars (FRMSs; Decressin et al. 2007b). In this scenario, later generation stars are expected to be formed by the gas ejected from earlier generation stars in the innermost region of a proto GC (Decressin et al. 2007a; D'Ercole et al. 2008; Vesperini et al. 2013). Therefore, the later generation stars would be observed to be more centrally concentrated than earlier generation stars unless this radial distribution was seriously affected by dynamical evolution (see, e.g., Miholics et al. 2015). This radial trend is indeed observed in many GCs, including ω Cen, M13, NGC 3201, NGC 6752, and 47 Tuc (Bellini et al. 2009; Kravtsov et al. 2010, 2011; Lardo et al. 2011; Nataf et al. 2011; Johnson & Pilachowski 2012; Milone et al. 2012). The incidence of spectroscopic binaries in different subpopulations, which is less affected by the dynamical evolution, also supports that later generation stars were formed in a denser environment where binaries are efficiently destroyed, resulting in a lower binary fraction for later generation stars (D'Orazi et al. 2010; Lucatello et al. 2015).

However, not every GC with multiple populations shows this general radial distribution trend. Carretta et al. (2010) and J.-W. Lee (2015) report a central concentration of metal-poor earlier generation stars in NGC 1851[1] and M22, respectively. These GCs are known as peculiar GCs showing intrinsic heavy elements dispersions (J.-W. Lee et al. 2009; Marino et al. 2009; Carretta et al. 2011; Lim et al. 2015), and therefore, their reversed radial trends may be considered to be the result of merging of two individual GCs (see Carretta et al. 2011). In the case of GCs without heavy elements spread, Dalessandro et al. (2014) have shown that two stellar populations in NGC 6362 share the same radial distribution, which is explained as a full spatial mixing accelerated by high mass loss rate of this GC (Miholics et al. 2015; see also Mucciarelli et al. 2016). Furthermore,

[1] Milone et al. (2009) showed that two stellar populations of subgiant branch stars in NGC 1851 share the same radial distribution, which, however, is contradicted by Carretta et al. (2011).

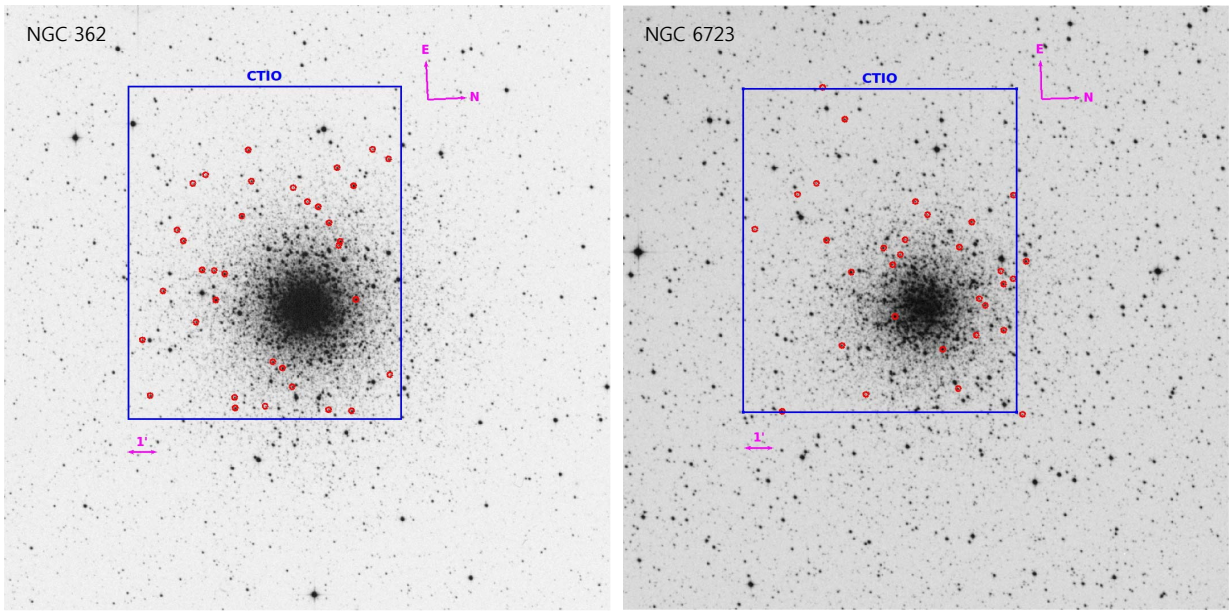

Figure 1. Our observed fields (blue squares) on the STScI images of NGC 362 and NGC 6723. The red circles indicate our spectroscopic target stars.

Larsen et al. (2015) recently suggested that first generation stars (primordial group) are more centrally concentrated than second generation stars (enriched group) in M15 using *Hubble Space Telescope* (*HST*) WFC3 photometry. This was not detected in the previous study for the same GC by Lardo et al. (2011) using the Sloan Digital Sky Survey (SDSS) data, which cover only the outer region of a cluster. Contrary to the cases of M22 and NGC 1851, the reversed radial trend in M15 is unlikely to be the result of merging, because this GC does not show Fe spread although variations in the light elements and some neutron-capture elements (Ba, Eu) were reported (Sneden et al. 1997; see also Bekki & Tsujimoto 2016). The spatial mixing due to dynamical evolution is also unlikely to explain this reversed radial trend (see, e.g., Vesperini et al. 2013). Therefore, the presence of a reversed radial distribution trend in M15 casts some doubt on the current self-enrichment scenario, and thus a search for further instances of this radial characteristic is required.

Investigating the radial distribution of multiple stellar populations, however, is not a simple task because spectroscopic observations are hard to secure a large enough number of samples and it is difficult to divide subpopulations using photometric observation alone. In this regard, our narrow-band photometry, combined with low-resolution spectroscopy, would be a useful tool for this investigation. Our previous studies have shown that narrow-band photometry using "Ca" and "Ca+CN" filters can efficiently detect multiple stellar populations with different chemical properties, and this is confirmed by low-resolution spectroscopy (Lim et al. 2015; Han et al. 2015). In this study, we have investigated the chemical properties and radial distributions of stars in NGC 362 and NGC 6723 by employing the same techniques and report that these two GCs show a central concentration of earlier generation stars, similarly to the case of M15.

Table 1. Mask Descriptions and Spectroscopic Observation Log

Object	Mask	No of stars	Exposures (N×s)
NGC 362	Bright	23	2×1200
			2×1500
	Faint	26	4×1500
NGC 6723	Bright	19	4×1200
			3×1500
	Faint	31	5×1500

2. NARROW-BAND PHOTOMETRY AND LOW-RESOLUTION SPECTROSCOPY

Our photometry was obtained at the Cerro Tololo Inter-American Observatory (CTIO) 4m Blanco telescope with "Ca+CN" filter in July 2009. As described in Lim et al. (2015), this filter was originally designed to measure only the strength of Ca II H&K lines, however, due to the deterioration, the filter passband was shifted to include CN molecular band at 3883 Å. Fortunately,

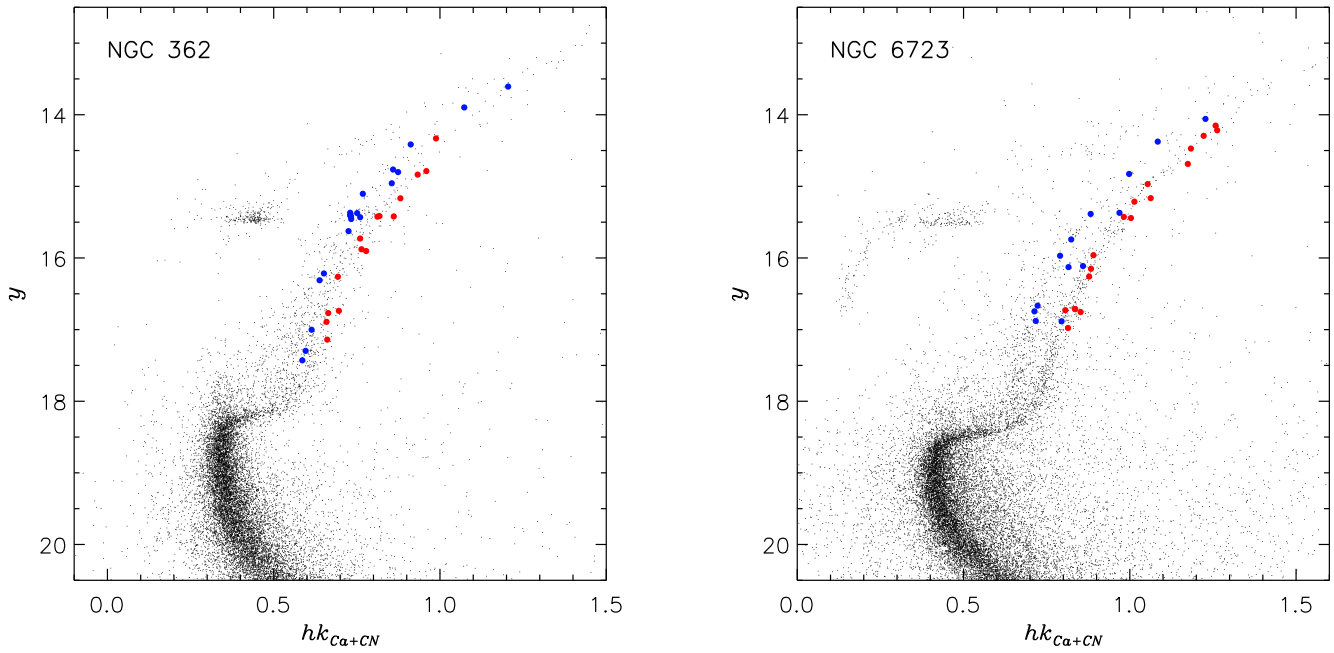

Figure 2. CMDs for NGC 362 (left) and NGC 6723 (right) in (y, hk_{Ca+CN}) plane obtained with the Ca+CN filter set at CTIO. Spectroscopic target stars are also identified in these CMDs, where the blue and red circles are CN-weak and red CN-strong stars, respectively (see Section 3). Note that RGB spread and split are shown in NGC 362 and NGC 6723, respectively.

this filter system became sensitive enough to detect the difference of CN band strength (see Hsyu et al. 2014; Lim et al. 2015), and this could therefore be effectively used to study multiple stellar populations with different CN abundances.

In this observation, we have used the MOSAIC II CCD Imager, which provides a pixel scale of 0.27″ and a field of view (FOV) of 36′ × 36′. However, only stars placed on chip 6 (FOV ∼ 9′ × 18′) are used for the analysis to avoid possible chip-to-chip variations of the mosaic CCDs (see Han et al. 2009; Roh et al. 2011). The observed fields are shown in Figure 1. Similarly to our previous works (Roh et al. 2011; Han et al. 2015; Lim et al. 2015), IRAF[2] MSCRED package and DAOPHOT II/ALLFRAME (Stetson 1987, 1994) were used for preprocessing and point spread function photometry. We also used CHI and SHARP parameters to exclude non-stellar objects and bad samples (i.e., CHI > 3.0, and SHARP > |1.0|). Note that, unlike our previous studies, the *sep* index was not used for sample selection in order to include stars in the central region of a cluster. Finally, astrometry was performed using the IRAF FINDER package with the 2MASS All-Sky Point Source catalog. Figure 2 shows color-magnitude diagrams (CMDs) for NGC 362 and NGC 6723 in (y, hk_{Ca+CN}[3]) plane. In these CMDs, NGC 362 shows a spread on the red giant-branch (RGB), and NGC 6723 shows two distinct RGBs, suggesting variations in CN band strength among RGB stars.

The spectroscopic data were obtained from Las Campanas Observatory (LCO) 2.5m duPont telescope in July 2011 and June 2014. We used Wide Field Reimaging CCD Camera (WFCCD) with HK grism, providing a dispersion of 0.8 Å/pixel and a central wavelength of 3700 Å. Two multi-slit masks were made for each GC using the CTIO photometry data, and at least four exposures were taken for each mask (see Table 1). For the data reduction, following Lim et al. (2015), the modified version of WFCCD reduction package and IRAF were used. More detailed information regarding observation and data reduction can be found in Lim et al. (2015) and Prochaska et al. (2006). We also measured the radial velocity of each star using the *rvidlines* task in IRAF RV package and estimated signal-to-noise (S/N) ratio at ∼3900 Å. From these parameters, non-member stars (radial velocity > 2.5σ of the mean velocity of each GC) and bad samples (S/N < 8) were excluded from our analysis. Finally, we have obtained spectra for 35 stars

[2] IRAF is distributed by the National Optical Astronomy Observatory, which is operated by the Association of Universities for Research in Astronomy (AURA) under a cooperative agreement with the National Science Foundation.

[3] We have used the same definition of the hk index defined by Anthony-Twarog et al. (1991), $hk = (\mathrm{Ca}-b) - (b-y)$. However, in this study, this index is expressed as hk_{Ca+CN} to clarify the difference of filter response function.

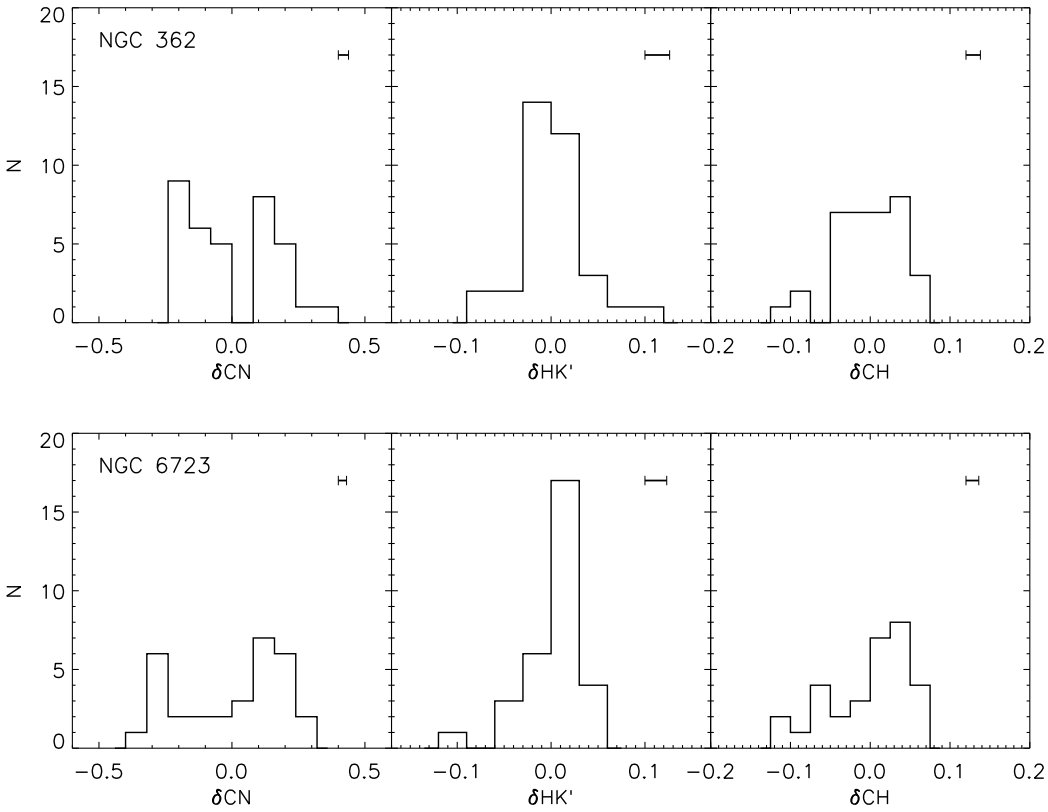

Figure 3. The histograms of δCN, δHK$'$, and δCH indices for RGB stars in NGC 362 (upper panels) and NGC 6723 (lower panels). The horizontal bar denotes the typical measurement error (1σ). Note that both GCs show the bimodal distribution in the δCN histogram.

in NGC 362, and 31 stars in NGC 6723, which are identified in Figures 1 and 2.

After the data reduction, we measured the CN, HK$'$, and CH indices for each star, which are defined by Harbeck et al. (2003) and Lim et al. (2015). The definitions for these indices are

$$\mathrm{HK}' = -2.5\log\frac{F_{3916-3985}}{2F_{3894-3911}+F_{3990-4025}},$$
$$\mathrm{CN}(3839) = -2.5\log\frac{F_{3861-3884}}{F_{3894-3910}},$$
$$\mathrm{CH4300} = -2.5\log\frac{F_{4285-4315}}{0.5F_{4240-4280}+0.5F_{4390-4460}},$$

where $F_{3916-3985}$, for example, is the integrated flux from 3916 to 3985 Å. In addition, delta indices (δCN, δHK$'$, and δCH) for each spectral index are also derived as the difference between the original index and the least squares fitting of the full sample in a GC (black solid lines in left panels of Figures 4 and 5) to reduce the effects of effective temperature ($T_{\rm eff}$) and surface gravity ($\log g$). The measured spectral indices are listed in Table 2.

3. MULTIPLE STELLAR POPULATIONS WITH DIFFERENT CN STRENGTHS

Since the early study by Smith (1984), several studies have reported variations in the CN and CH molecular bands among stars in NGC 362 (Kayser et al. 2008; Smith & Langland-Shula 2009). More recent studies found Na-O anti-correlation, suggesting multiple stellar populations (Carretta et al. 2013; see also Shetrone & Keane 2000), but no evidence for heavy elements spread was reported for this GC (Worley & Cottrell 2010). Spectroscopic studies for NGC 6723, however, are relatively rare. Gratton et al. (2015) have shown the presence of multiple stellar populations in this GC from the Na-O anti-correlation among horizontal branch (HB) stars. Rojas-Arriagada et al. (2016) report chemical abundances for only a few RGB stars. In order to investigate the chemical properties of RGB stars in NGC 362 and NGC 6723 from our spectroscopy, we have plotted histograms of δCN, δHK$'$, and δCH indices respectively in Figure 3. These two GCs show clear bimodal distributions in the δCN index, whereas they show unimodal and narrow distributions in the δHK$'$ index. For the δCH index, although there are no significant separations, standard deviations of the distributions (0.04 for NGC 362; 0.05 for NGC 6723) are much larger than the typical measurement errors ($\sim$0.017) in both GCs. The presence of bimodal CN distribution in NGC 362 is con-

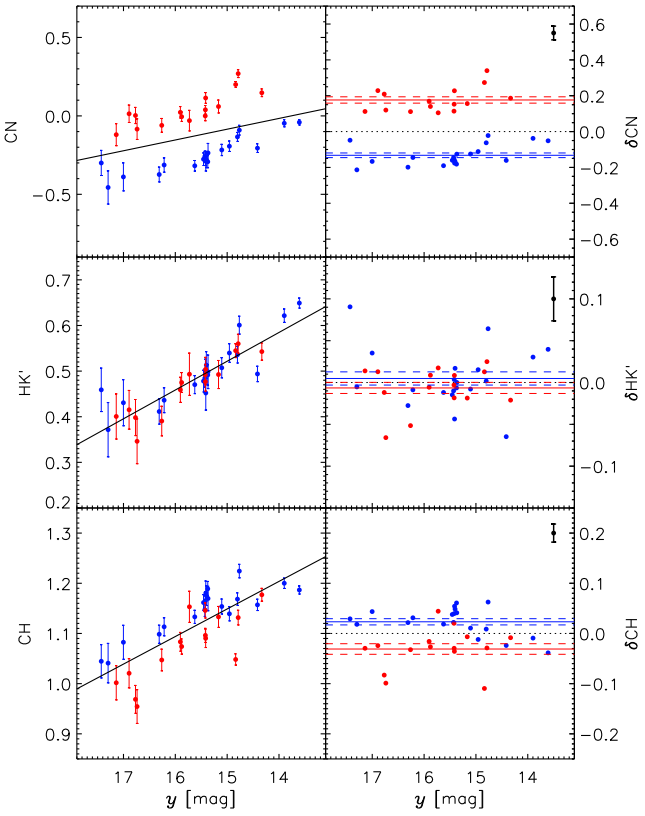

Figure 4. Left panels: Measured spectral indices (CN, HK′, and CH) as functions of y magnitude for RGB stars in NGC 362, where the blue and red circles are CN-weak and CN-strong stars. Right panels: The δCN, δHK′, and δCH indices plotted against y magnitude. The mean value and the error of the mean ($\pm1\sigma$) for each subpopulation are denoted by solid and dashed lines, respectively. The vertical bars in the upper right corner denote the typical measurement error for each index. Note that the two subpopulations are clearly separated in the δCN and δCH indices, but not in the δHK′ index. In addition, the strengths of the CN and CH bands are anti-correlated.

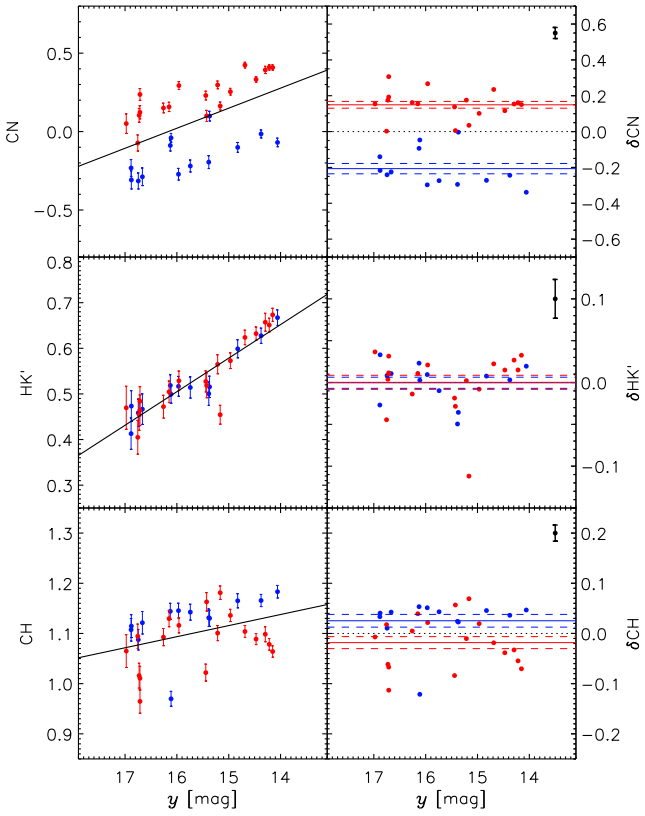

Figure 5. Same as Figure 4, but for NGC 6723. Note that this GC shows similar trends as NGC 362, such as CN bimodality and CN-CH anti-correlation.

sistent with earlier findings by Smith (1984) and Smith & Langland-Shula (2009). While the CN bimodality in NGC 6723 was not reported previously from spectroscopic observations, Smith & Hesser (1986) found some hints of CN variation from DDO photometry.

For more comprehensive analysis, we have divided observed RGB stars into CN-strong (δCN $\geq$ 0.0) and CN-weak (δCN $<$ 0.0) stars for both GCs. We note that CN-strong and CN-weak stars are clearly separated in our photometry (see Figure 2), indicating that RGB spread and split in these GCs are due to the difference in CN band strength. Figures 4–5 compare the strengths of measured spectral indices between CN-strong and CN-weak subpopulations for NGC 362 and NGC 6723, respectively. We note that CN, HK′, and CH indices are affected by temperature and gravity, and therefore, we have compared the mean strengths of two subpopulations on the δ-index diagrams (see Section 2). These two GCs show fairly similar trends in every spectral index. First of all, as shown in the histogram of Figure 3, CN-strong and CN-weak stars are clearly separated in δCN index versus y magnitude diagram. The differences between the two subpopulations are 0.31 for NGC 362, and 0.36 for NGC 6723, which are significant at 14.1σ and 10.4σ levels respectively, compared to the standard deviation of the mean for each group. This difference for NGC 362 is comparable to that discovered in previous studies (Smith 1984; Smith & Langland-Shula 2009). In case of the δHK′ index, however, the mean values of the two subpopulations are almost identical to within the standard error. Lastly, the CN-weak stars are more enhanced in the CH band than CN-strong stars, implying the presence of CN-CH anti-correlation, which is a well-known feature in many GCs (e.g., Harbeck et al. 2003; Pancino et al. 2010; Smolinski et al. 2011). For the δCH index, the two subpopulations are separately by 0.054 (4.4σ) for NGC 362, and 0.044 (2.5σ) for NGC 6723. Our results thus indicate that NGC 362 and NGC 6723 show abundance variations in the light elements (C, N), but not in the heavy element (Ca). These observations, together with the presence of Na-O anti-correlation and the absence of Fe spread in these GCs (Worley & Cottrell 2010; Carretta et al. 2013; Gratton et al. 2015), suggest that they belong to the "normal" GCs with multiple stellar populations.

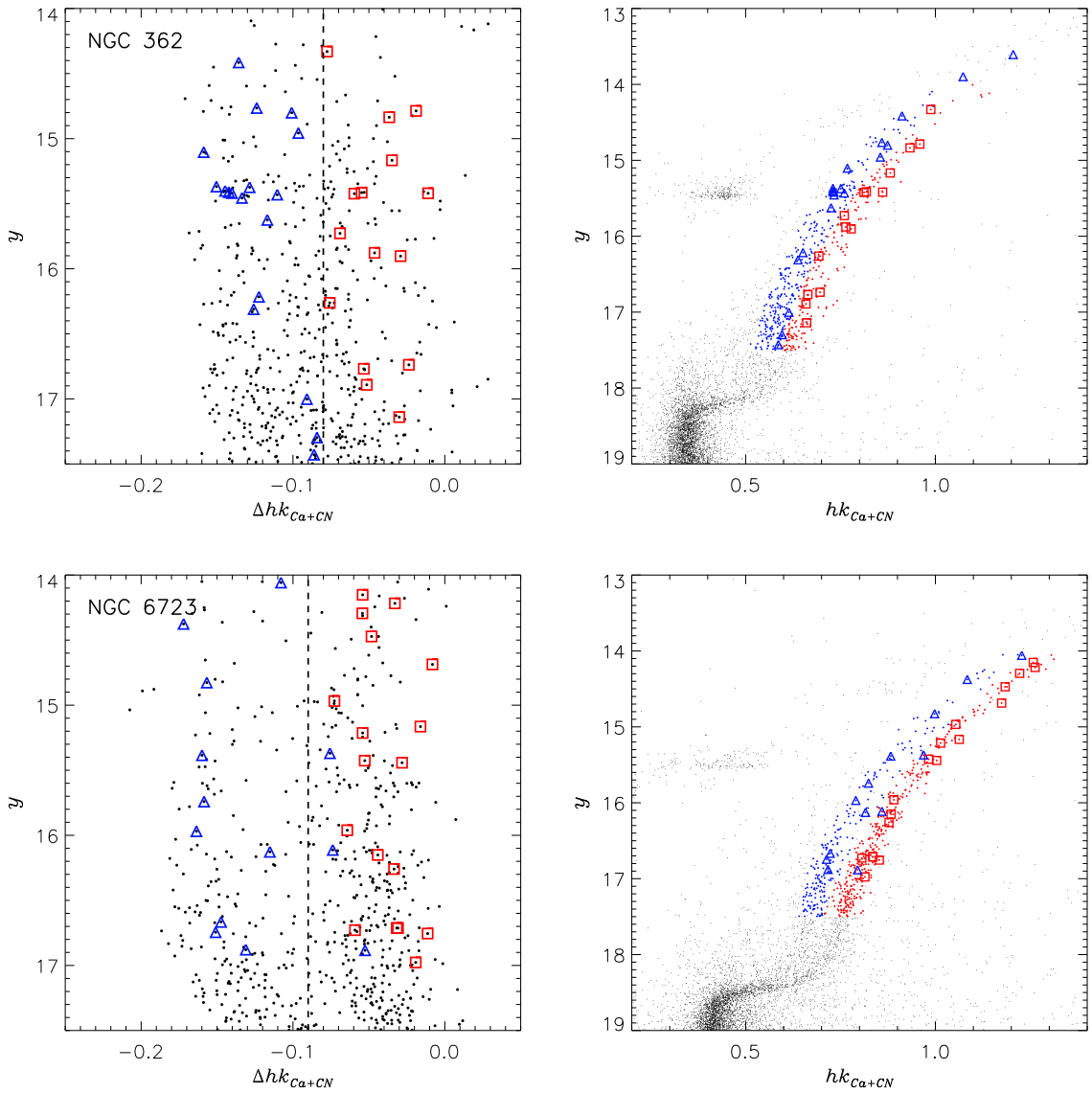

Figure 6. Left panels: The RGB stars in NGC 362 (upper) and NGC 6723 (lower) are plotted in the (y, Δhk_{Ca+CN}) diagram. The blue triangles and the red squares represent CN-weak and CN-strong stars, respectively, identified from our low-resolution spectroscopy. We divided all RGB stars ($14.0 < y < 17.5$) into two subpopulations, CN-weak and CN-strong, by Δhk_{Ca+CN}=-0.08 (dashed line) for NGC 362 and Δhk_{Ca+CN}=-0.09 for NGC 6723. Right panels: The two subpopulations are plotted on the (y, hk_{Ca+CN}) CMD for each GC, where the blue and red points are CN-weak and CN-strong stars, respectively.

4. RADIAL DISTRIBUTIONS OF MULTIPLE STELLAR POPULATIONS

In our low-resolution spectroscopy, observed RGB stars in NGC 362 and NGC 6723 are clearly divided into two subpopulations by CN index, and these subpopulations are also well separated in (y, hk_{Ca+CN}) CMDs (see Figure 2). However, the number of spectroscopic stars for each GC is limited to only ∼30, and we have therefore divided subpopulations using Ca+CN filter photometry in order to secure enough stars to investigate the radial distribution of stellar populations. First of all, we have plotted (y, Δhk_{Ca+CN}) diagrams for the RGB stars including our spectroscopic samples, in the left panels of Figure 6, where the Δhk_{Ca+CN} index is determined from the difference between the hk_{Ca+CN} index and the right-edge line of RGB for each GC. Only RGB stars in the $14.0 < y < 17.5$ magnitude range have been used for this analysis. We have excluded bright stars ($y > 14.0$) to avoid a possible evolutionary mixing effect, and faint stars ($y < 17.5$) due to the absence of spectroscopic samples in this magnitude range. As shown in these figures, CN-weak (blue triangles) and CN-strong (red squares) stars, classified from our low-resolution spectroscopy, are also well separated in these diagrams. Therefore, we divided all RGB stars, observed from Ca+CN filter photometry, into CN-weak and CN-strong subpopulations at Δhk_{Ca+CN}=-0.08 for NGC 362, and Δhk_{Ca+CN}=-0.09 for NGC 6723. These

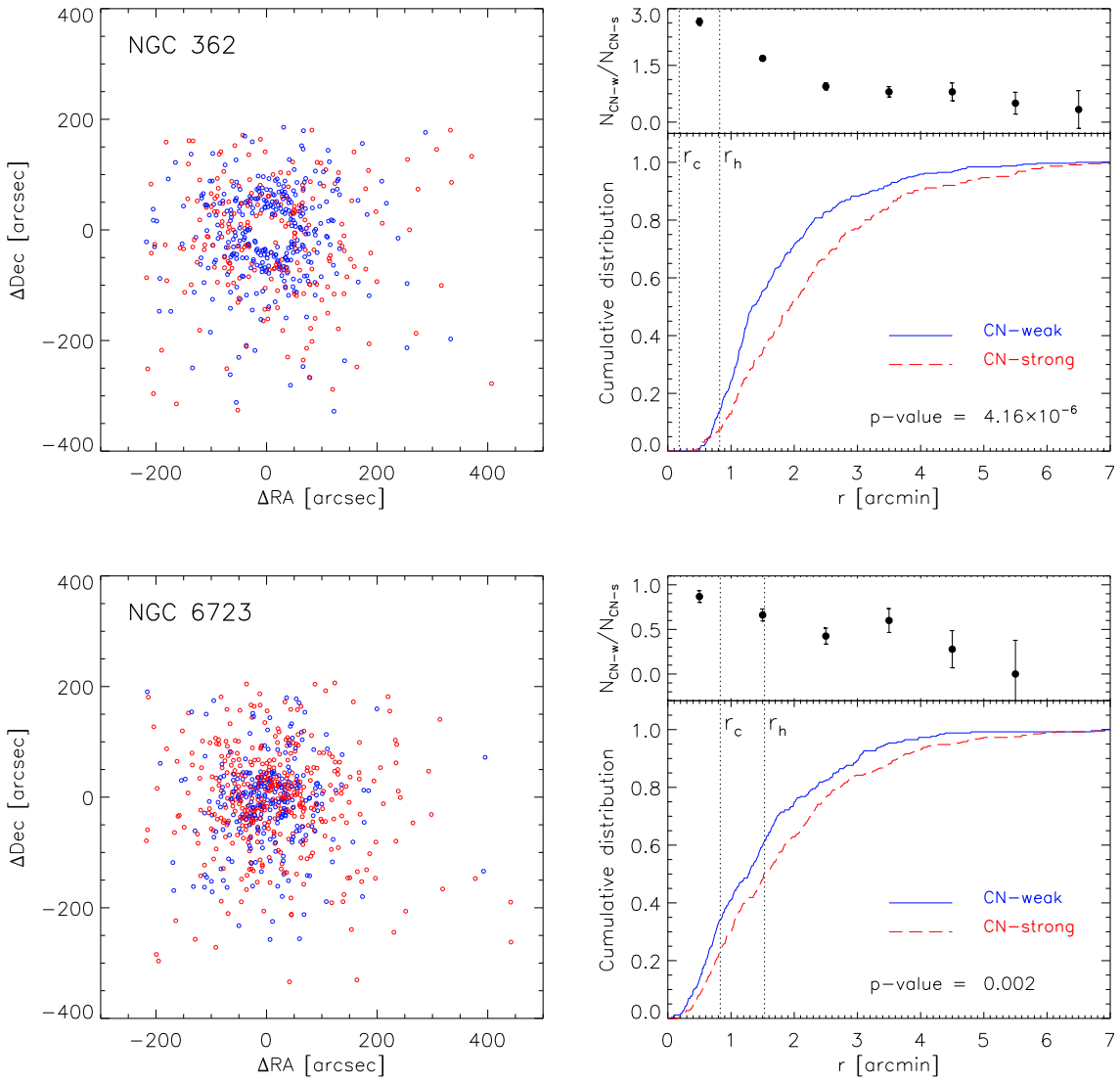

Figure 7. Spatial (left panels) and cumulative (right panels) distributions of RGB stars in NGC 362 and NGC 6723, together with number ratio between CN-weak and CN-strong stars as a function of distance from the center. The blue and red open circles are CN-weak and CN-strong RGB stars identified in the right panels of Figure 6. We note that stars placed on the cluster center of NGC 362 ($r < 0.5'$) are excluded by CHI and SHARP parameters (see text). For both GCs, CN-weak earlier generation stars (blue) are more centrally concentrated than CN-strong later generation stars (red). The p-value for NGC 362 is only 4.16×10^{-6}, indicating that the two subpopulations have definitely different radial distributions. In the case of NGC 6723, the p-value is 0.002, which is somewhat larger than that of NGC 362, but still significant. Vertical dotted lines in right panels mark the core and half-light radii (Harris 2010).

subpopulations are marked on the CMDs in the right panels of Figure 6. The number ratio between CN-weak (blue) and CN-strong (red) stars is estimated to be 0.38:0.62 for NGC 6723 (from 597 stars), and 0.59:0.41 for NGC 362 (from 538 stars). The fraction of enriched subpopulation (CN-strong stars) for NGC 6723 is similar to the general trend of GCs (∼0.68; see Bastian & Lardo 2015), although there is some difference in the definition of enriched subpopulation.

Figure 7 shows the spatial distribution (left panels) and the cumulative distribution of each subpopulation (right panels) for RGB stars in NGC 362 and NGC 6723, respectively, together with the number ratio between CN-weak and CN-strong stars as a function of distance from the center. The stars placed on the cluster center of NGC 362 ($r < 0.5'$) are excluded by CHI and SHARP parameters due to the severe contamination by adjacent starlight (see Section 2). In this figure, the CN-weak stars (blue) are more centrally concentrated than the CN-strong stars (red) in NGC 362, and the number ratio decreases with increasing distance from the center. In general, CN-weak stars are considered to be earlier generation stars, and therefore, this result is contrary to the fact that many GCs show a central con-

centration of later generation stars (see Section 1). In order to verify the difference in radial distribution between the two subpopulations, we have performed the Kolmogorov-Smirnov (KS) test. The probability-value (p-value) is only 4.16×10^{-6} with a maximum deviation of 0.22 for NGC 362. This result thus indicates that these two subpopulations definitely have different radial distributions. NGC 6723 also shows a central concentration of CN-weak earlier generation stars. The KS test indicates the p-value of 0.002 and the deviation of 0.15, confirming that the two subpopulations show different radial distributions. When we divide RGB stars into three subpopulations, CN-weak, CN-intermediate, and CN-strong, the central concentration of CN-weak subpopulation becomes more clear in both GCs.

Carretta et al. (2013, hereafter C13), however, report an apparently different result for the radial distribution of stars in NGC 362. In their high-resolution spectroscopy, the second generation stars (intermediate and extreme components) show a more centrally concentrated distribution than the first generation stars (primordial component), where primordial, intermediate, and extreme components are defined from the Na-O anti-correlation. As described by them, however, the level of confidence for the radial distribution is not very high due to the small sample size (N=71). The p-value[4] is 0.2730, which is much larger than the value from our result (4.16×10^{-6}). On the other hand, it is important to check the definition of subpopulations in the two studies, because we have divided the two subpopulations by CN index, whereas C13 was based on [Na/Fe] abundance. In the upper panel of Figure 8, we have compared our δCN index with [Na/Fe] abundance of C13 for 12 common spectroscopic stars. They show a strong correlation, which is in good agreement with previous studies for other GCs (Sneden et al. 1992; Marino et al. 2008), indicating that the subgrouping of our study is not significantly different from that of C13.

The number ratio between the earlier and later generation stars obtained from this study for NGC 362 is also different from that suggested by C13. The fraction of CN-weak earlier generation stars estimated from our Ca+CN photometry is ∼0.59, while that of primordial component stars from C13 is only ∼0.22. In the lower panel of Figure 8, we have cross-matched stars of C13 on the (y, hk_{Ca+CN}) CMD to find the origin of this difference. As shown in this CMD, most of the bright stars ($y < 14.0$) in C13 are classified as the later generation, but our study excluded these stars from the analysis to avoid a possible evolutionary mixing effect. Therefore,

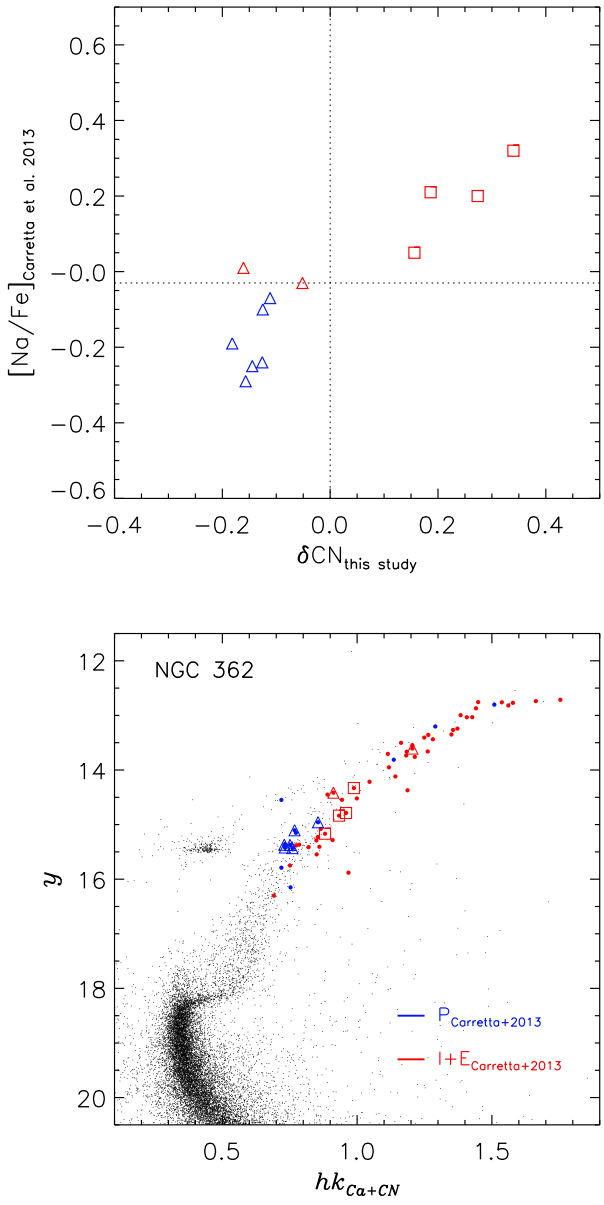

Figure 8. Comparison between our study and C13 for NGC 362. Upper panel: The [Na/Fe] abundance from C13 plotted against the δCN index of this study for 12 common stars. We note that they show a strong correlation and similar subgrouping. The blue and red colors represent the first (primordial) and second (intermediate and extreme) generation stars, divided by [Na/Fe], and triangles and squares indicate the CN-weak and CN-strong stars, divided by δCN index. Dotted lines denote the criteria of each study (δCN=0.0; [Na/Fe]=-0.03). Lower panel: C13 stars are identified on the (y, hk_{Ca+CN}) CMD, where the blue and red circles are the first and second generation stars, respectively. It is important to note that most of the bright stars ($y < 14.0$) in C13 are defined as the second generation, while these stars are excluded in our study (see text).

the different results between the two studies might be due to the classification of these bright stars. However, for more rigorous comparison, it is required to investigate the correlation between stellar populations divided by CN index and those divided in the Na-O plane.

[4] "KS-probability" in C13.

5. DISCUSSION

We have shown that the RGB stars in NGC 362 and NGC 6723 are clearly divided into two subpopulations by CN index, but these two subpopulations show no difference in calcium abundance from our low-resolution spectroscopy. The well-known CN-CH anti-correlation between the two subpopulations is also shown in both GCs. These results, together with previous findings by other investigators (Worley & Cottrell 2010; Carretta et al. 2013; Gratton et al. 2015), suggest that these two GCs are "normal" GCs with multiple stellar populations. Furthermore, we found that the CN-weak earlier generation stars are significantly more centrally concentrated than CN-strong later generation stars in both GCs. These findings are important as the second and third cases that show such a reversed radial distribution trend, following M15 by Larsen et al. (2015). We note, however, that the innermost region ($r < 0.5'$) of a cluster was not included in our analysis for NGC 362, and therefore further analysis with the recent HST UV survey (Piotto et al. 2015) would be helpful to confirm the reversed spatial distribution discovered in this study.

As described in Section 1, the self-enrichment scenario predicts more centrally concentrated stars belonging to the later generation (see, e.g., Vesperini et al. 2013). Therefore, our finding of centrally concentrated CN-weak earlier generation stars in NGC 362 and NGC 6723 is not generally acceptable in this framework. The merging of two individual GCs might be a possible solution for different radial distributions of stellar populations (see Carretta et al. 2011), but these GCs do not show additional evidence of merging, such as metallicity difference. Moreover, their chemical properties, the bimodal CN distribution and CN-CH anti-correlation without Fe spread, are not intuitively understandable in the merging scenario. Larsen et al. (2015) suggested that mass segregation may explain the observed radial trend of M15. This scenario, however, requires extreme He enhancement of later generation stars ($Y \geq 0.40$) in order to produce a mass difference of $0.25 M_{\odot}$, which is not observed in this GC. In either case of NGC 362 and NGC 6723, He enhancement is not yet reported, although some ΔY is expected. Therefore, the mass segregation by the difference in He abundance alone is not likely to explain the observed radial trends in M15, NGC 362, and NGC 6723. More recently, an alternative solution for the mass difference is proposed by Henault-Brunet (2015), which suggests that the different incidence of binary from primordial and enriched stellar populations may provoke this required mass difference (see also Hong et al. 2015). According to them, this effect is more efficient in more concentrated GCs. Interestingly, M15 has been known as a core collapsed GC, and NGC 362 and NGC 6723 are also classified as possible core collapsed GCs (Harris 2010). The effects of mass segregation on the radial distribution of stellar generations require more detailed studies. To this end, we plan to run direct N-body simulations of NGC 362 and NGC 6723 (Pasquato et al. in prep.) under different assumptions for the relevant binary fractions, initial concentration of the second generation stars, and mass-difference between the subpopulations to assess to what extent mass-segregation can explain our findings in these GCs. At this stage, it is worth noting that the half-mass relaxation time of NGC 362 is relatively short (less than 1Gyr) while that of NGC 6723 is roughly of the same order of that of M15 (∼2Gyr). Therefore, we expect that mass-segregation would play a more important role in the former cluster.

One caveat in this analysis is that definitions of subpopulations are not exactly identical in many studies. We have divided stars in a GC into two subpopulations by the strength of the CN band, whereas many high-resolution spectroscopic studies based on Na and O abundances prefer to separate them into three subpopulations (Carretta et al. 2009; Johnson & Pilachowski 2012). In addition, Jang et al. (2014) and Jang & Lee (2015) suggest the presence of three subpopulations with different He abundances based on population models for RR Lyrae and HB stars. As shown in our previous study (Lim et al. 2015), CN-weak stars in NGC 1851 could be further divided into two subpopulations, and therefore, it is possible that CN-weak stars in other GCs also might be further divided into two subgroups. This issue will be discussed in our forthcoming paper.

We are grateful to the anonymous referee for a number of helpful suggestions. Support for this work was provided by the National Research Foundation of Korea to the Center for Galaxy Evolution Research, and by KASI under the R&D program (Project No. 2014-1-600-05) supervised by the Ministry of Science, ICT and future Planning. M.P. acknowledges support from Mid-career Researcher Program (No. 2015-008049) through the National Research Foundation (NRF) of Korea.

REFERENCES

Anthony-Twarog, B. J., Twarog, B. A., Laird, J. B., & Payne, D. 1991, AJ, 101, 1902

Bastian, N., & Lardo, C. 2015, MNRAS, 453, 357

Bekki, K., & Tsujimoto, T. 2016, arXiv:1608.08012

Bellini, A., Piotto, G., Bedin, L. R., et al. 2009, A&A, 507, 1393

Carretta, E., Bragaglia, A., Gratton, R. G., et al. 2009, A&A, 505, 117
Carretta, E., Bragaglia, A., Gratton, R. G., et al. 2013, A&A, 557, A138 (C13)
Carretta, E., Gratton, R. G., Lucatello, S., et al. 2010, ApJL, 722, L1
Carretta, E., Lucatello, S., Gratton, R. G., Bragaglia, A., & D'Orazi, V. 2011, A&A, 533, A69
Dalessandro, E., Massari, D., Bellazzini, M., et al. 2014, ApJL, 791, L4
Decressin, T., Charbonnel, C., & Meynet, G. 2007, A&A, 475, 859
Decressin, T., Charbonnel, C., Siess, L., et al. 2009, A&A, 505, 727
Decressin, T., Meynet, G., Charbonnel, C., Prantzos, N., & Ekström, S. 2007, A&A, 464, 1029
de Mink, S. E., Pols, O. R., Langer, N., & Izzard, R. G. 2009, A&A, 507, L1
D'Ercole, A., Vesperini, E., D'Antona, F., McMillan, S. L. W., & Recchi, S. 2008, MNRAS, 391, 825
D'Orazi, V., Gratton, R., Lucatello, S., et al. 2010, ApJL, 719, L213
Gratton, R. G., Carretta, E., & Bragaglia, A. 2012, A&A Rv, 20, 50
Gratton, R. G., Lucatello, S., Sollima, A., et al. 2015, A&A, 573, A92
Han, S.-I., Lee, Y.-W., Joo, S.-J., et al. 2009, ApJL, 707, L190
Han, S.-I., Lim, D., Seo, H., & Lee, Y.-W. 2015, ApJL, 813, L43
Harbeck, D., Smith, G. H., & Grebel, E. K. 2003, AJ, 125, 197
Harris, W. E. 2010, arXiv:1012.3224
Henault-Brunet, V. 2015, IAU General Assembly, 22, 2252802
Hong, J., Vesperini, E., Sollima, A., et al. 2015, MNRAS, 449, 629
Hsyu, T., Johnson, C. I., Lee, Y.-W., & Rich, R. M. 2014, PASP, 126, 597
Jang, S., & Lee, Y.-W. 2015, ApJS, 218, 31
Jang, S., Lee, Y.-W., Joo, S.-J., & Na, C. 2014, MNRAS, 443, L15
Johnson, C. I., & Pilachowski, C. A. 2012, ApJL, 754, L38
Kayser, A., Hilker, M., Grebel, E. K., & Willemsen, P. G. 2008, A&A, 486, 437
Kravtsov, V., Alcaíno, G., Marconi, G., & Alvarado, F. 2010, A&A, 512, L6
Kravtsov, V., Alcaíno, G., Marconi, G., & Alvarado, F. 2011, A&A, 527, L9
Lardo, C., Bellazzini, M., Pancino, E., et al. 2011, A&A, 525, A114
Larsen, S. S., Baumgardt, H., Bastian, N., et al. 2015, ApJ, 804, 71
Lee, J.-W., Kang, Y.-W., Lee, J., & Lee, Y.-W. 2009, Nature, 462, 480
Lee, J.-W. 2015, ApJS, 219, 7
Lim, D., Han, S.-I., Lee, Y.-W., et al. 2015, ApJS, 216, 19
Lucatello, S., Sollima, A., Gratton, R., et al. 2015, A&A, 584, A52
Marino, A. F., Milone, A. P., Piotto, G., et al. 2009, A&A, 505, 1099
Marino, A. F., Sneden, C., Kraft, R. P., et al. 2011, A&A, 532, A8
Marino, A. F., Villanova, S., Piotto, G., et al. 2008, A&A, 490, 625
Miholics, M., Webb, J. J., & Sills, A. 2015, MNRAS, 454, 2166
Milone, A. P., Piotto, G., Bedin, L. R., et al. 2012, ApJ, 744, 58
Milone, A. P., Stetson, P. B., Piotto, G., et al. 2009, A&A, 503, 755
Mucciarelli, A., Dalessandro, E., Massari, D., et al. 2016, arXiv:1604.04151
Nataf, D. M., Gould, A., Pinsonneault, M. H., & Stetson, P. B. 2011, ApJ, 736, 94
Pancino, E., Rejkuba, M., Zoccali, M., & Carrera, R. 2010, A&A, 524, A44
Piotto, G., Milone, A. P., Bedin, L. R., et al. 2015, AJ, 149, 91
Prochaska, J. X., Weiner, B. J., Chen, H.-W., & Mulchaey, J. S. 2006, ApJ, 643, 680
Roh, D.-G., Lee, Y.-W., Joo, S.-J., et al. 2011, ApJL, 733, L45
Rojas-Arriagada, A., Zoccali, M., Vásquez, S., et al. 2016, A&A, 587, A95
Shetrone, M. D., & Keane, M. J. 2000, AJ, 119, 840
Smith, G. H. 1984, AJ, 89, 1545
Smith, G. H., & Hesser, J. E. 1986, PASP, 98, 838
Smith, G. H., & Langland-Shula, L. E. 2009, PASP, 121, 1054
Smolinski, J. P., Martell, S. L., Beers, T. C., & Lee, Y. S. 2011, AJ, 142, 126
Sneden, C., Kraft, R. P., Prosser, C. F., & Langer, G. E. 1992, AJ, 104, 2121
Sneden, C., Kraft, R. P., Shetrone, M. D., et al. 1997, AJ, 114, 1964
Stetson, P. B. 1987, PASP, 99, 191
Stetson, P. B. 1994, PASP, 106, 250
Ventura, P., & D'Antona, F. 2008, MNRAS, 385, 2034
Vesperini, E., McMillan, S. L. W., D'Antona, F., & D'Ercole, A. 2013, MNRAS, 429, 1913
Worley, C. C., & Cottrell, P. L. 2010, MNRAS, 406, 2504

Table 2. Index Measurements for the sample stars in NGC 362 and NGC 6723

ID	Ra	Dec	y	hk_{Ca+CN}	HK′	errHK′	δHK′	CN	errCN	δCN	CH	errCH	δCH
N362-1003	15.82759	-70.89803	13.8980	1.0730	0.6215	0.0147	0.0304	-0.0471	0.0228	-0.0379	1.2000	0.0104	-0.0093
N362-1005	15.70891	-70.86282	14.4150	0.9120	0.4938	0.0170	-0.0648	-0.2056	0.0272	-0.1609	1.1570	0.0113	-0.0239
N362-1009	15.87088	-70.89255	14.7650	0.8590	0.6008	0.0196	0.0643	-0.0910	0.0311	-0.0222	1.2243	0.0135	0.0626
N362-1014	15.91741	-70.82832	15.1040	0.7680	0.5073	0.0221	-0.0078	-0.2171	0.0360	-0.1250	1.1537	0.0149	0.0106
N362-1019	15.92921	-70.91448	15.3690	0.7300	0.4985	0.0368	0.0001	-0.2362	0.0606	-0.1260	1.1697	0.0245	0.0412
N362-1020	16.02489	-70.87573	15.3740	0.7510	0.4916	0.0225	-0.0065	-0.2922	0.0384	-0.1816	1.1890	0.0147	0.0608
N362-1022	15.79167	-70.90933	15.4020	0.7300	0.5133	0.0293	0.0170	-0.2802	0.0503	-0.1677	1.1753	0.0196	0.0486
N362-1023	15.84620	-70.92680	15.4120	0.7310	0.4520	0.0376	-0.0436	-0.2891	0.0623	-0.1758	1.1804	0.0241	0.0542
N362-1024	15.72000	-70.86794	15.4190	0.7320	0.4988	0.0274	0.0036	-0.2705	0.0462	-0.1568	1.1654	0.0183	0.0396
N362-1028	15.94930	-70.83397	15.4560	0.7330	0.4782	0.0239	-0.0147	-0.2764	0.0400	-0.1601	1.1615	0.0158	0.0378
N362-1529	15.81924	-70.82098	14.3310	0.9880	0.5428	0.0189	-0.0211	0.1474	0.0246	0.1863	1.1771	0.0129	-0.0084
N362-2003	16.00982	-70.81965	13.6070	1.2050	0.6492	0.0110	0.0397	-0.0406	0.0174	-0.0514	1.1866	0.0080	-0.0386
N362-2011	15.63266	-70.82576	14.7870	0.9590	0.5600	0.0207	0.0249	0.2696	0.0251	0.3399	1.1316	0.0147	-0.0289
N362-2012	15.96672	-70.88182	14.8010	0.8740	0.5360	0.0182	0.0018	-0.1339	0.0285	-0.0626	1.1684	0.0124	0.0087
N362-2014	16.04104	-70.82831	14.8360	0.9330	0.5448	0.0152	0.0128	0.2000	0.0190	0.2736	1.0482	0.0111	-0.1096
N362-2017	15.64483	-70.88963	14.9570	0.8550	0.5397	0.0203	0.0153	-0.1934	0.0332	-0.1114	1.1392	0.0141	-0.0120
N362-2025	15.67090	-70.93616	15.1670	0.8810	0.4925	0.0308	-0.0186	0.0599	0.0411	0.1563	1.1330	0.0208	-0.0066
N362-2038	15.87910	-70.90480	15.4150	0.8180	0.5039	0.0263	0.0085	0.1143	0.0340	0.2277	1.0903	0.0184	-0.0357
N362-2039	16.07741	-70.87669	15.4200	0.8610	0.4768	0.0205	-0.0183	0.0389	0.0274	0.1527	1.0962	0.0140	-0.0295
N362-2040	15.97682	-70.83964	15.4230	0.8120	0.4920	0.0224	-0.0030	-0.0000	0.0311	0.1139	1.1459	0.0150	0.0203
N362-2041	16.05219	-70.79980	15.4310	0.7600	0.4845	0.0199	-0.0100	-0.2590	0.0330	-0.1445	1.1472	0.0133	0.0221
N362-3006	15.63587	-70.83836	16.2160	0.6510	0.4362	0.0273	-0.0088	-0.3131	0.0457	-0.1446	1.1133	0.0181	0.0312
N362-3007	15.91064	-70.82910	16.3110	0.6380	0.4114	0.0276	-0.0276	-0.3737	0.0474	-0.1987	1.0984	0.0181	0.0216
N362-4004	15.66253	-70.88970	15.6250	0.7250	0.4703	0.0197	-0.0119	-0.3182	0.0338	-0.1903	1.1331	0.0132	0.0186
N362-4009	15.76517	-70.93929	15.7280	0.7600	0.4932	0.0463	0.0174	-0.0302	0.0657	0.1047	1.1531	0.0310	0.0443
N362-4015	15.67688	-70.85783	15.8780	0.7640	0.4750	0.0218	0.0087	-0.0052	0.0300	0.1401	1.0739	0.0151	-0.0266
N362-4017	15.94820	-70.91762	15.9030	0.7780	0.4590	0.0275	-0.0057	0.0227	0.0368	0.1697	1.0834	0.0188	-0.0158
N362-4033	15.87707	-70.89821	16.2620	0.6930	0.3905	0.0325	-0.0515	-0.0603	0.0441	0.1113	1.0471	0.0216	-0.0323
N362-4060	16.06938	-70.80835	16.7380	0.6960	0.3462	0.0492	-0.0659	-0.0844	0.0658	0.1199	0.9544	0.0337	-0.0990
N362-4062	15.98650	-70.84545	16.7690	0.6640	0.3982	0.0395	-0.0119	0.0026	0.0516	0.2091	0.9687	0.0278	-0.0830
N362-4072	15.69080	-70.80397	16.8920	0.6590	0.4152	0.0424	0.0129	0.0135	0.0556	0.2285	1.0207	0.0292	-0.0242
N362-4088	16.02500	-70.90798	17.0020	0.6140	0.4306	0.0505	0.0352	-0.3890	0.0893	-0.1665	1.0825	0.0338	0.0436
N362-4109	16.03894	-70.90070	17.1400	0.6610	0.4006	0.0495	0.0139	-0.1198	0.0704	0.1122	1.0017	0.0341	-0.0295
N362-4138	16.01084	-70.85294	17.2970	0.5960	0.3716	0.0595	-0.0052	-0.4562	0.1060	-0.2135	1.0409	0.0393	0.0182
N362-4162	15.64587	-70.87316	17.4290	0.5860	0.4590	0.0477	0.0905	-0.3001	0.0801	-0.0482	1.0445	0.0332	0.0291
N6723-1004	284.85938	-36.62233	14.3757	1.0840	0.6275	0.0167	0.0031	-0.0150	0.0256	-0.2439	1.1656	0.0121	0.0362
N6723-1007	284.86337	-36.67758	15.3852	0.8823	0.5005	0.0257	-0.0496	-0.1947	0.0410	-0.2946	1.1313	0.0175	0.0242
N6723-1026	284.91367	-36.67157	14.0584	1.2275	0.6672	0.0170	0.0195	-0.0693	0.0276	-0.3386	1.1832	0.0125	0.0467
N6723-1029	284.92978	-36.65347	14.8267	0.9979	0.5989	0.0198	0.0077	-0.1008	0.0316	-0.2720	1.1651	0.0141	0.0456
N6723-2001	284.81909	-36.71124	14.2177	1.2627	0.6510	0.0150	0.0150	0.4101	0.0175	0.1611	1.0783	0.0116	-0.0546
N6723-2002	284.83209	-36.61426	15.2139	1.0138	0.5649	0.0208	0.0022	0.2973	0.0247	0.1756	1.1007	0.0150	-0.0102
N6723-2017	284.87149	-36.58863	14.9679	1.0537	0.5728	0.0172	-0.0080	0.2545	0.0212	0.1013	1.1359	0.0122	0.0195
N6723-2025	284.88257	-36.64808	14.2945	1.2221	0.6571	0.0196	0.0268	0.3931	0.0232	0.1539	1.0984	0.0150	-0.0328
N6723-2037	284.90323	-36.58818	14.1520	1.2579	0.6734	0.0144	0.0326	0.4082	0.0171	0.1508	1.0640	0.0114	-0.0704
N6723-2044	284.91840	-36.57550	14.4722	1.1837	0.6322	0.0145	0.0149	0.3329	0.0176	0.1164	1.0888	0.0110	-0.0385
N6723-2048	284.93604	-36.68473	14.6869	1.1745	0.6238	0.0160	0.0223	0.4239	0.0181	0.2349	1.1039	0.0119	-0.0186
N6723-2050	284.94626	-36.60479	15.4423	1.0034	0.5273	0.0230	-0.0186	0.2299	0.0279	0.1373	1.0220	0.0170	-0.0839
N6723-2051	284.96124	-36.63554	15.4265	0.9820	0.5186	0.0270	-0.0285	0.0999	0.0356	0.0054	1.1630	0.0183	0.0567
N6723-2052	284.96408	-36.58178	15.3696	0.9689	0.5155	0.0234	-0.0357	0.0985	0.0310	-0.0033	1.1302	0.0161	0.0227

Table 2 continued

Table 2 *(continued)*

ID	Ra	Dec	y	hk_{Ca+CN}	HK′	errHK′	δHK′	CN	errCN	δCN	CH	errCH	δCH
N6723-2054	285.01886	-36.67313	15.1647	1.0628	0.4544	0.0207	-0.1119	0.1629	0.0251	0.0349	1.1812	0.0133	0.0692
N6723-3001	284.81351	-36.57934	16.1273	0.8157	0.5186	0.0235	0.0231	-0.0885	0.0352	-0.0935	1.1441	0.0161	0.0534
N6723-3003	284.82947	-36.66508	16.8789	0.7171	0.4734	0.0337	0.0331	-0.3082	0.0577	-0.2172	1.1146	0.0228	0.0405
N6723-3046	284.88876	-36.59848	15.7411	0.8238	0.5142	0.0232	-0.0098	-0.2194	0.0381	-0.2738	1.1424	0.0158	0.0432
N6723-3063	284.90668	-36.58289	15.9691	0.7903	0.5167	0.0217	0.0095	-0.2719	0.0371	-0.2971	1.1454	0.0148	0.0512
N6723-3073	284.91208	-36.58960	16.7448	0.7132	0.4585	0.0301	0.0084	-0.3149	0.0511	-0.2411	1.0876	0.0204	0.0105
N6723-3091	284.95197	-36.62900	16.6659	0.7227	0.4666	0.0334	0.0107	-0.2883	0.0562	-0.2245	1.1214	0.0224	0.0425
N6723-4045	284.86853	-36.60382	16.7289	0.8062	0.4552	0.0349	0.0039	0.1034	0.0441	0.1752	1.0160	0.0247	-0.0615
N6723-4077	284.89359	-36.60166	15.9613	0.8906	0.5287	0.0214	0.0210	0.2933	0.0250	0.2671	1.1161	0.0150	0.0217
N6723-4121	284.91809	-36.64885	16.1128	0.8593	0.4993	0.0197	0.0027	-0.0401	0.0282	-0.0470	0.9698	0.0149	-0.1213
N6723-4124	284.92496	-36.64448	16.7130	0.8357	0.4640	0.0335	0.0115	0.1229	0.0421	0.1927	1.0108	0.0239	-0.0670
N6723-4128	284.92929	-36.61201	16.1512	0.8832	0.5046	0.0237	0.0108	0.1575	0.0297	0.1555	1.1295	0.0162	0.0393
N6723-4131	284.93518	-36.64169	16.2592	0.8777	0.4721	0.0250	-0.0137	0.1503	0.0309	0.1621	1.0928	0.0171	0.0049
N6723-4136	284.94473	-36.72401	16.9771	0.8143	0.4696	0.0471	0.0366	0.0509	0.0625	0.1544	1.0649	0.0327	-0.0070
N6723-4148	284.96790	-36.70012	16.7123	0.8349	0.4840	0.0320	0.0315	0.2367	0.0377	0.3064	0.9647	0.0238	-0.1131
N6723-4153	284.97528	-36.68954	16.8838	0.7949	0.4130	0.0345	-0.0269	-0.2320	0.0536	-0.1404	1.1074	0.0225	0.0334
N6723-4162	285.04105	-36.68499	16.7548	0.8521	0.4049	0.0371	-0.0445	-0.0728	0.0513	0.0023	1.0944	0.0243	0.0175